Chapter 2

pO_2 and ROS/RNS Measurements in the Microcirculation in Hypoxia

Silvia Bertuglia and Marcos Intaglietta

Abstract

We expose methods for in vivo assessment of oxygen, nitric oxide (NO), and reactive oxygen species (ROS)/reactive nitrogen species (RNS), in the microcirculation during normoxia and hypoxia. We provide an example of the related mechanisms of ROS/RNS and oxygen level in the process of regulating capillary perfusion. Namely, we discuss the real time pO_2 measurements in vivo in the microvessels and tissues of the hamster cheek pouch and window chamber preparations during normoxia and hypoxia, as well as the corresponding changes in ROS/RNS in systemic blood during normoxia and hypoxia under conditions where NO availability is maximally reduced.

Key words: Nitric oxide, Oxidative stress, Oxygen, Arterioles, Microcirculation, Blood perfusion

1. Introduction

The assessment of oxygen tension (pO_2) and reactive oxygen species (ROS)/ reactive nitrogen species (RNS) play a crucial role in a multitude of physiological and pathologic conditions. Initially, ROS/RNS were thought to be primarily cytotoxic species that increased tissue injury (1). Conversely, they can be endogenously produced and are essential in the immune response and in many physiological signal transduction pathways (2). There are several ROS that can be generated in the body organs: superoxide anion (O_2^-), hydrogen peroxide (H_2O_2), hydroxyl radicals (OH^-), nitric oxide (NO), peroxynitrite ($ONOO^-$) and others (3–5). NO is the most important in the homeostatic regulation of the immune, cardiovascular, and nervous system (6). The formation of RNS is not an inescapable consequence of synthesizing NO. It is efficiently removed by oxyhemoglobin to form nitrate, which prevents even the highest

D. Armstrong (ed.), *Advanced Protocols in Oxidative Stress II*, Methods in Molecular Biology, vol. 594
DOI 10.1007/978-1-60761-411-1_2,

rates on NO synthesis from directly reacting with oxygen to form a significant amount of nitrogen dioxide. However, the simultaneous activation of superoxide synthesis along with NO will completely transform the biological action of NO by forming peroxynitrite.

There are several mechanisms for NO consumption, including red blood cell reactions, cellular metabolism, and reaction with ROS. Interestingly, most consumptive mechanisms of NO are O_2-dependent according to the metabolic state of the cell. Oxygen is a major substrate that regulates the rate of NO synthesis because change in pO_2 has a profound influence on NO synthase activity. The production of NO from arginine by the synthase requires molecular oxygen. Oxygen dependency is one of the major differences between the NOS isoforms, neuronal (NOS-1), endothelial (NOS-3), and the inducible NOS-2. NO inhibits the mechanism of O_2 consumption in tissues and mitochondrial respiration and therefore, increases in NO will increase O_2 which will, in turn, further increase NOS activity (7). Moreover, cellular NO consumption is O_2 dependent and proportional to oxygen concentration; as the O_2 level increases, so does the rate of NO metabolism (8). Taken together, we see that there is a close relationship between these two gases, which is critical in the regulation of tissue oxygenation and perfusion (9–12). Autoregulatory mechanisms that adjust the diameter of arterioles and blood perfusion to the oxygen demand of tissues have become a cornerstone of vascular pathophysiology. There is substantial evidence to suggest that oxygen reactivity is mediated, at least in part, by the oxygen-dependent production of vasoconstrictors, likely in addition to the production of vasodilators during severe hypoxia (9). The formation of NO-derived S-nitrosothiols (RSNOs) can stimulate guanylate cyclase, and thereby promote vasorelaxation (13). S-nitrosohemoglobin adducts are also involved in oxygen delivery (14).

A major challenge is the development of specific and sensitive methods for measuring pO_2 and quantifying ROS/RNS in cells and tissues. The measurement of pO_2 and transport at the microcirculatory level is technically difficult because of limited accessibility and the necessity of high-resolution techniques to differentiate between arterioles, venules, capillaries, and tissues within the microcirculation (15–19). Blood pO_2 has also been evaluated by measurements of light absorption at different wavelengths of the hemoglobin absorption spectrum (20–24). Mass spectrometry is also invasive and employs a relatively large tissue probe, yielding an "average" rather than a localized measurement (25). The quenching method, based on the relationship between the decay rate of excited phosphorescence from palladium-mesotetra-(4-carboxyphenyl) porphyrin bound to albumin, enables pO_2 measurement in the blood and the tissue as the probe passes to the interstitium according to the exchange of albumin from blood to tissue.

A commonly used approach measures markers of ROS/RNS rather than the actual radical. These markers of oxidative stress are measured using a variety of different assays. Lipid peroxidation has been and remains one of the most widely used indicators of oxidant/free radical formation in vitro and in vivo. Oxidants such as hydroxyl radicals, peroxyl radicals, nitrogen dioxide, peroxynitrite, and higher oxidation states of heme and hemoproteins (ferryl heme) are capable of initiating and propagating peroxidation of polyunsaturated fatty acids, thereby degrading membrane lipids (26).

Unfortunately, many of the methods used to detect lipid peroxidation in urine, blood plasma, or tissue are nonspecific, relying on the detection of thiobarbituric acid (TBA)-reactive substances such as malondialdehyde (MDA) or other reactive aldehydes generated from the in vivo or ex vivo decomposition of lipid peroxidation products (27). However, a variety of different bio-organic substances (e.g., bile acids, carbohydrates, nucleic acids, certain antibiotics, and amino acids) react with TBA to varying degrees, rendering this method sensitive, but not very specific. Elevated MDA levels have been measured in virtually every organ in experimental models of septic shock, hemorrhagic shock, and ischemia/reperfusion injury, where the role of peroxynitrite has been attested by various antiperoxynitrite strategies, such as melatonin (28–31). A particularly useful method is to measure F_2-like prostanoid derivatives of arachidonic acid, termed F_2-isoprostanes (IsoP) (32).

The detection of RSNO has often employed the Saville reaction, which involves the displacement of the nitrosonium ion (NO^+) by mercury salts. The resulting nitrite or NO generated from the spontaneous decomposition of NO^+ is detected by methods such as chemiluminescence or HPLC. Other techniques for the detection of RSNO employ colorimetric methods such as the Griess reaction to measure the nitrite formed from the treatment of RSNO with mercuric chloride. However, samples that contain large amounts of nitrite can interfere with and limit the detection range of these methods under acidic conditions. To overcome these problems, two methods have been devised to detect RSNO-derived nitrosating species at neutral pH (33). The colorimetric method uses the components of the Griess reaction while the fluorimetric method uses the conversion of DAN to its fluorescent triazole derivative (34). These methods may be conducted at neutral rather than acidic pH, eliminating the interference of contaminating nitrite and allowing the detection of nitrosation mediated by the presence of NO. Lipid peroxidation and the formation of peroxyl radicals and aldehydes damage membranes, membrane-bound enzymes, and receptors. Protein damage may result in their unfolding, fragmentation, and polymerization, while damage to DNA can cause mutations or enzyme activation.

Clinically, the evaluation of this type of ROS generation is limited by the very short half life (e.g., nanoseconds) of these free radicals (5).

In addition, ROS can be measured using electron spin resonance (ESR), also termed electron paramagnetic resonance spectroscopy and the spin trapping method(35). This technique and nuclear magnetic resonance spectroscopy are based on the magnetic properties of unpaired electrons and their molecular environment. These unpaired electrons exist in two orientations, either parallel or antiparallel with respect to an applied magnetic field. The energy differences of these states correspond to the microwave region of the electromagnetic spectrum. Although unpaired electrons of species such as NO, OH, or O_2^- are too low in concentration and too short-lived to be directly detected by ESR in biological systems, this dilemma can be circumvented by the ESR measurement of more stable secondary radical species formed by adding exogenous spin-traps, molecules that react with the primary radical species to give longer-lasting radical adducts with characteristic ESR signatures, which can accumulate to levels permitting detection. Interestingly, this spin-trap approach can also be used to measure tissue oxygen consumption and to noninvasively map spatially localized oxygen concentrations in living tissues. (36). Although instability, tissue metabolism, the sometimes broad reactivity of spin traps, and the cost of ESR spectrometers can be problematic, when combined with parallel strategies for detecting specific reactive species, ESR has proven to be a useful and revealing free radical detection strategy (37). However, these methods involve equipment and expertise not always found in most laboratories.

A major challenge is the development of specific and sensitive methods for measuring pO_2 and quantifying ROS/RNS in cells and tissues. This chapter provides an important example of the related mechanisms of ROS/RNS and oxygen level in the process of regulating capillary perfusion. In what follows, we discuss pO_2 measurements in vivo in microvessels and tissues of the hamster cheek pouch and window chamber preparations (38–44) during normoxia and hypoxia, as well as the corresponding changes in ROS/RNS in systemic blood during normoxia and hypoxia under conditions where NO availability is maximally reduced.

2. Materials

2.1. Equipment

1. Mean arterial blood pressure (MAP)-Heart rate: Viggo-Spectramed P10E2 transducer, Oxnard, CA, USA; Gould Windograf recorder, Mod. 13-6615-10S Gould Inc. Ohio, USA.

2. p_AO_2, p_ACO_2, pH: Blood Chemistry Analyzer 248, Bayer, Norwood, MA.
3. Blood Viscosity: Brookfield, Middleboro, MA.
4. *Hematocrit*. Hettick Hct 20 Centrifuge; Tuttlingen, Germany.
5. *Intravital microscopy*. Orthoplan, Leica Microsystem GmbH, Wetzlar, Germany.
6. *Charge-couple device camera*. COHU 4815-2000, San Diego CA.
7. *Videocassette recorder*. Panasonic AG-7355, Tokyo, Japan.
8. *Sony monitor*. PMV-1271Q, Tokyo, Japan.
9. *Red blood cell velocity*. Photo Diode/Velocity Tracker Model 102B, Vista Electronics, San Diego, CA.
10. *Fluorescence decay-curve fitter*. Model 802, Vista Electronics, Ramona, CA.
11. Potentiostat and Keithley Electrometer-Amplifier model 610C, Cleveland, OH.

3. Reagents and Supplies

1. 2-phenyl-4,4,5,5-tetramethylimidazoline-1-oxyl-3-oxide (carboxy-PTIO, CPTIO: Cayman Chemical, Michigan USA).
2. Palladium-meso-tetra(4-carboxyphenyl)porphyrin: Porphyrin Products, Inc., Logan, UT.
3. Analytic method d-ROMs: Diacron s.r.l., Parma Italy.
4. Thiobarbituric acid reactive kit: TBARS, ZeptoMetric, Corp. Buffalo, NY, USA.
5. Aliphatic alcohols Sigma-Aldrich, St Louis, MO.

4. Methods

4.1. Hamster Cheek Pouch Preparation

4.1.1. Systemic Parameters

Male Syrian hamsters (80–100 g, Charles River, Italy) *were anesthetized* by pentobarbital sodium, 50 mg/kg/intraperitoneally injected. Animal handling and care are according to the procedures approved by the Animal Care and Use Committee at the Italian Research Council. The right carotid artery and left femoral vein are cannulated for measurements of blood pressure and arterial blood gases, and the administration of drugs, respectively. Mean arterial blood pressure (MAP) and heart rate (HR) are

acquired continuously during the experiment[1]. Arterial and venous blood is sampled from the catheter in the carotid artery and jugular vein into heparinized capillary tubes and analyzed for pO_2, pCO_2, pH[2], hematocrit[3], hemoglobin[4] at 37°C. A decrease of the fraction of inspired oxygen (FIO_2) is induced by normobaric hypoxia (10 O_2, FIO_2 0.1, balance N_2). Between each oxygen level, the animal is allowed 10 min to stabilize before the data acquisition. The groups are subjected to systemic parameters, blood gas analysis, and pO_2 measurements during baseline and after 20 min of exposure to hypoxia. Two groups are infused intravenously with the NO scavenger, the nitronyl nitroxide compound oxidized and reduced form of 2-phenyl-4,4,5,5-tetramethylimidazoline-1-oxyl-3-oxide (carboxy-PTIO, CPTIO, 1.0 mg/Kg, 10 mg/ml solution) or the vehicle (isotonic saline). CPTIO reacts stechiometrically with NO to generate NO_2 and a 2-carboxyphenyl-4,4,5,5-tetramethylimidazoline-1-oxyl (PTI) derivative. CPTIO is water soluble and has been shown to have very strong NO-scavenging properties based on a radical-radical reaction with NO (12). The cheek pouch is spread out over a Plexiglas microscope stage and a region of about 1 cm^2 in area is prepared as a single layer (9). The cheek pouch is covered with transparent plastic film to prevent both desiccation of the tissue and gas exchange with the atmosphere. Observations are made with an intravital microscope[5]. All selected microvessels and interstitial tissue segments are recorded by a video camera[6] displayed on a monitor[7] and transferred to a video recorder[8]. The hamster's body temperature and cheek pouch temperature are maintained at 37°C with circulating warm water. Baseline characterization (systemic hemodynamics, blood sampling for TBARS and nitrite/nitrate measurements, arteriolar diameter, RBC velocity) is performed after a 30 min stabilization period. Arterioles are chosen for investigation and followed throughout the protocol.

4.2. Dorsal Skin Fold Window Chamber Preparation

4.2.1. Systemic Parameters

Investigations are performed in 55–65 g male Golden Syrian Hamsters fitted with a dorsal window chamber. Animal handling and care follows the NIH Guide for the Care and Use of Laboratory Animals. Catheters are tunneled under the skin, exteriorized at the dorsal side of the neck, and securely attached to the window frame. MAP and HR are recorded continuously[1]. Hematocrit is measured from centrifuged arterial blood samples taken in heparinized capillary tubes[4]. Arterial blood is collected in heparinized glass capillaries (50 µl) and immediately analyzed for p_AO_2, p_ACO_2, base excess (BE), and pH[2]. The unanesthetized animal is placed in a restraining tube with a longitudinal slit from which the window chamber protrudes, then fixed to the microscopic stage for transillumination with the intravital microscope[5]. Animals are given 20 min to adjust to the tube environment before any measurement is carried out. The tissue image is projected onto a charge-coupled device camera[6] connected to a

videocassette recorder[8] and viewed on a monitor[7]. Measurements are carried out using a 40× (NA 0.8) water immersion objective. The same sites of study are followed throughout the experiment, so that comparisons to baseline levels could be made directly. A decrease of the fraction of inspired oxygen (FIO_2) is induced by normobaric hypoxia (10 O_2, FIO_2 0.1, balance N_2). Between each oxygen level, the animal is allowed 10 min to stabilize before the data acquisition. The groups are subjected to systemic parameters, blood gas analysis, and pO_2 measurements during baseline and after 20 min of exposure to hypoxia. Two groups are infused intravenously with CPTIO (1.0 mg/kg, 10 mg/ml solution) or the vehicle (isotonic saline) (12)

4.3. Measurement of Microvascular Parameters

4.3.1. Microhemodynamics

Arteriolar and blood flow velocities are measured on-line by using the photodiode cross-correlation method. The measured centerline velocity (V) is corrected according to vessel size to obtain the mean RBC velocity[9]. A video image-shearing method is used to measure the vessel diameter (D). Blood flow (Q) is calculated from the measured values as $Q=\pi\times V(D/2)^2$. Changes in arteriolar diameter from the baseline are used as indicators of a change in the vascular tone (40, 41).

4.3.2. Functional Capillary Density

Functional capillaries, defined as those capillary segments that have an RBC transit of at least a single RBC in a 45 s period in ten successive microscopic fields, were assessed in a region totaling 0.46 mm^2. Each field had between two and five capillary segments with RBC flow. Functional capillary density (FCD) (cm^{-1}), i.e., the total length of the RBC perfused capillaries divided by the area of the microscopic field of view, was evaluated by measuring and adding the length of the capillaries that had an RBC transit in the field of view. The relative change in FCD from the baseline levels after each intervention is indicative of the extent of capillary perfusion (41, 42)

4.3.3. Measurement of Microvascular pO_2

Phosphorescence quenching microscopy is based on the oxygen-dependent quenching of phosphorescence emitted by an albumin-bound metalloporphyrin complex after pulsed light excitation (*see* Note 1). The phosphorescence quenching microscopy is independent of the dye concentration within the tissue and is well suited for detecting hypoxia because its decay time is inversely proportional to the pO_2 level, causing the method to be more precise at low pO_2. The phosphorescence decay curves are converted to oxygen tension using a fluorescence decay-curve fitter. This technique has been used in this animal and others for both intravascular and extravascular oxygen tension measurements. Tissue pO_2 measurements are possible in this preparation because the albumin-bound dye equilibrates between the plasma and tissue compartments as a consequence of the increased permeability of the

subcutaneous connective and adipose tissue to albumin. The animals receive a slow intravenous injection of 15 mg/kg bw at a concentration of 10.1 mg/ml of a palladium-meso-tetra(4-carboxyphenyl) porphyrin. The dye is allowed to circulate for 20 min before pO_2 measurements are carried out(12, 15). The phosphorescence is excited by pulsed light (30 Hz, 4 µs duration) for a period of <5 s, and intravascular measurements are made by placing an optical rectangular window (5 × 15 µm) within the vessel of interest with the longest side of the rectangular slit positioned parallel to the vessel wall. Tissue pO_2 is measured in regions void of large vessels within intracapillary spaces (10 × 10 µm) (24). In the present configuration of the oxygen measuring system, tissue pO_2 values are obtained with a repeatability of 1–3 Torr capturing the emission from a tissue area of 75–100 μm^2 (43). The phosphorescence decay curves are converted to oxygen tensions using a fluorescence decay curve fitter. Measurements in regions with large tissue gradients in the vicinity of arterioles are made using a shaping list in a rectangular format, which is placed along the outside of the vessel wall, and by varying the length at which the acceptable signal-to-noise ratio was obtained (44). Perivascular pO_2 measurements are made by placing the centerline of the measuring slit at a distance of one-tenth of the diameter of the inner vessel that stops at the blood tissue interface (*see* Notes 2–3).

4.3.4. Measurement of Lipid Peroxides (ROS)

4.3.4.1. Analytical

This section describes the analytic method d-ROMs (39, 40) to measure plasma hydroperoxides, based on Fenton's reaction or on radical formation during lipid peroxidation. The oxyradical species produced, which is directly proportional to the amount of plasma peroxides, is trapped by alchylamine, a phenolic compound that forms a coloured stable radical detectable spectrophotometrically at 505 nm. The concentration of the coloured complex is directly correlated to the concentration of the hydroperoxides. Ten µl of a chromogenic substance and 1 ml of the kit buffer are mixed with 10 µl of blood for 1 min at 37°C. The results are expressed in arbitrary units (a.u.; 1 a.u. = 0.08 mg/100 ml H_2O_2). Blood samples are taken at the baseline and after hypoxia from the cannulated carotid artery.

4.3.4.2. TBARS

Lipid peroxidation is also measured in plasma using an assay to estimate the levels of thiobarbituric acid reactive substances. TBARS, including mainly lipid peroxides and malondialdehyde, generated during the peroxidative process are determined using 100 µl of plasma and 60 min incubation under acidic conditions at 96°C, via spectrophotometric measurements at 532 nm. TBARS values are expressed in terms of malondialdehyde equivalents as nmol/ml.

4.3.5. NO Measurements

4.3.5.1. Electrodes

Perivascular NO levels were measured using amperiometric bi-polymer coated (Nafion and *o*-phenylenediamine) carbon fiber microelectrodes. The electrodes were fabricated by sequential dipping and drying in Nafion (5% in aliphatic alcohols). They were additionally coated with 5 mM *o*-phenylenediamine dihydrocholoride (1, 2-benzenediame solution), which selectively repels ascorbic acid and dopamine (45). The current generated was measured with a potentiostat and an electrometer-amplifier[11]. The sensitivity of each electrode to ascorbic acid was evaluated by measuring its response to a 30 mM solution equilibrated with 100% Argon and compared to the magnitude of the response to 1 nM of NO. The electrodes selected for use in these studies had less than a 2% response to ascorbic acid. NO sensitivity was of 7 nM. The stability of the electrodes was re-assessed after the measurements by repeating the calibration procedure. Data from the electrodes outside the defined characteristics or presenting calibration changes greater than 5% were discarded from the study. Measurements were made in the perivascular space, in the abluminal side of the microvascular walls to obtain an estimate of the NO level in the vascular smooth muscle. This required removing the window chamber cover glass and superfusing the tissue (~5 ml/min) with heated physiological Krebs salt solution equilibrated with 95% N_2 and 5% CO_2, which maintained the suffusate at pH 7.4. The fluid was dripped onto the tissue to maintain a 35–36°C temperature and minimize oxygen delivery to the tissue. NO measurements began 20 min after the removal of the window to allow the tissue to stabilize and the microvascular hemodynamics to return to baseline levels (46). Measurements were made by penetrating the tissue with the NO electrode maneuvered with a micromanipulator and the tip positioned as close as possible to the microvessel without touching the wall, as this stimulation causes transient and sustained changes in NO concentration (47–49).

4.3.5.2. Griess Reaction

One method for the indirect determination of NO involves the spectrophotometric measurement of its stable decomposition products NO_3^- and NO_2^-. This method requires that NO_3^- first be reduced to NO_2^- and then NO_2^- determined by the Griess reaction (50). This reaction is a two step-diazotization reaction in which the NO derived nitrosating agent (e.g. N_2O_3) generated from the acid-catalyzed formation of nitrous acid from nitrite (or the interaction of NO with oxygen), reacts with sulfanilic acid to produce a diazonium ion that is then coupled to *N*-(1-napthyl) ethylediamine to form a chromophoric azo product that absorbs strongly at 543 nm. Briefly, blood samples are centrifuged, separated from RBCs, and the plasma is stored at –70°C. After ultrafiltration of the plasma through a 10-kDa membrane, the samples are incubated with nitrate reductase and enzyme cofactors for 3 h

for conversion of nitrate to nitrite. Absorbance is read at 543 nm using a plate reader after addition of the Griess reagents that convert nitrite into a deep purple azo compound.

All reported values are means ± (SD). (GraphPad Software, Inc., San Diego California USA) was used to analyze statistical differences. The data were analyzed by the Mann Witney test to examine the differences between the groups. The Friedman two way analysis of variance by ranks test was used to determine the differences between the groups at different times. Where significant differences were indicated by this test, a further comparative analysis was undertaken using the Dunn's test. Data were presented as absolute values and ratios, as relative to the baseline values. A ratio of 1.0 would signify no change from the baseline, whereas lower and higher ratios are indicative of changes proportionally lower and higher than the baseline (i.e. 1.5 would mean a 50% increase from the baseline level). All measurements were compared with the baseline levels obtained before the experimental procedure. Differences are considered significant at $P < 0.05$.

4.3.6. Results

4.3.6.1. Hamster Cheek Pouch

4.3.6.1.1. Systemic Parameters and Microhemodynamics

Twenty animals were used for the study; ten received a continuous infusion of the NO scavenger and ten, a continuous infusion of the vehicle. Table 2.1 summarizes the changes in the systemic parameter response to hypoxia that caused significant changes in blood pO_2, pCO_2, and pH. These changes are the consequence of hyperventilation, a normal response to hypoxia. The microvascular diameter and blood flow responses to hypoxia with and without CPTIO are shown in Fig. 2.1a. CPTIO reduced the diameter of the arterioles in normoxia. Hypoxia resulted in a statistically significant vasodilation. CPTIO and hypoxia maintained a significant vasoconstriction. The continuous infusion of the NO scavenger significantly reduced FCD to 0.95 (SD 0.07) of the normoxic baseline [1.35 (SD 0.08), $P < 0.05$]. Hypoxia resulted in a decrease in FCD [0.90 (SD 0.05)] for the vehicle. CPTIO and hypoxia further decreased FCD [0.68 (SD 0.07), $P < 0.05$] , which was significantly lower than normoxia and hypoxia without the NO scavenger.

4.3.6.1.2. Microvascular Oxygen Distribution

Figure 2.2a shows the distribution of pO_2 in the arterioles and in the interstitial space for normoxia and hypoxia with and without the NO scavenger. During normoxia, CPTIO decreased the intravascular pO_2. Tissue pO_2 was significantly reduced with CPTIO when compared with normoxic animals. With CPTIO and hypoxia, the intravascular pO_2 was similar and lower than during hypoxia in the arterioles.

4.3.6.1.3. ROS/RNS Measurements

CPTIO significantly increased ROS formation vs. normoxic animals (Fig. 2.3) Hypoxia significantly increased ROS formation compared with normoxia. Nitrate/nitrite concentrations in the plasma were significantly increased after hypoxia and reduced after CPTIO (Fig. 2.4).

Table 2.1
Systemic parameters during normoxia and hypoxia with and without the treatment with NO scavenger in hamster skin fold and in hamster cheek pouch

	Cheek pouch normoxia	Cheek pouch hypoxia	Skin fold window normoxia	Skin fold window hypoxia
	(n = 10)	(n = 10)	(n = 6)	(n = 6)
MAP (mmHg)				
Vehicle	88.3 ± 5	86.5 ± 7	103 ± 5	105 ± 7
Treatment	98.4 ± 4*°	92.5 ± 6*	149 ± 8*	128 ± 7*
HR (beats/min)				
Vehicle	320 ± 12	330 ± 10	418 ± 23	468 ± 41
Treatment	350 ± 10	360 ± 10	470 ± 39	489 ± 27
paO_2, (Torr)				
Vehicle	70.8 ± 5.4	29.3 ± 2.7*	60.4 ± 7.2	27.4 ± 3.2*
Treatment	68.3 ± 7.2	30.5 ± 3.5*	67.8 ± 6.2	30.5 ± 8.8*
$paCO_2$, (Torr)				
vehicle	59.4 ± 4.2	36.3 ± 2.4*	53.7 ± 6.4	33.4 ± 3.2*
Treatment	53.3 ± 3.5	32.5 ± 3.2*	44.6 ± 5.4*	30.2 ± 5.4*
Arterial pH				
Vehicle	7.36 ± 0.02	7.48 ± 0.03*	7.35 ± 0.02	7.47 ± 0.02
Treatment	7.38 ± 0.03	7.49 ± 0.02*	7.38 ± 0.03	7.48 ± 0.04

The mean blood pressure (MAP), heart rate (HR), pO_2, arterial pO_2–pCO_2. Values are means ±SE. *n* no of animals
* $P < 0.05$ vs. normoxia

4.3.6.2. Skin Fold Window Preparation

4.3.6.2.1. Systemic Parameters and Microhemodynamics

Twelve animals were used for the study; six received a continuous infusion of CPTIO and six, the continuous infusion of the vehicle. Table 2.1 summarizes the changes in the systemic parameter response to hypoxia. The continuous infusion of the NO scavenger during normoxia induced a significant arteriolar vasoconstriction ratio (Fig. 2.1b). Hypoxia resulted in a statistically significant increase in the diameter of the arterioles. CPTIO and hypoxia maintained significant arteriolar vasoconstriction. Diameter and RBC velocity data were used to compute the microvascular blood flow in each vessel studied (Fig. 2.1b). Continuous infusion of the NO scavenger during normoxia induced a statistically significant reduction of FCD to 0.78 (SD 0.09) of the baseline. Hypoxia resulted in a small decrease in FCD [0.94 (SD 0.08)] for the vehicle.

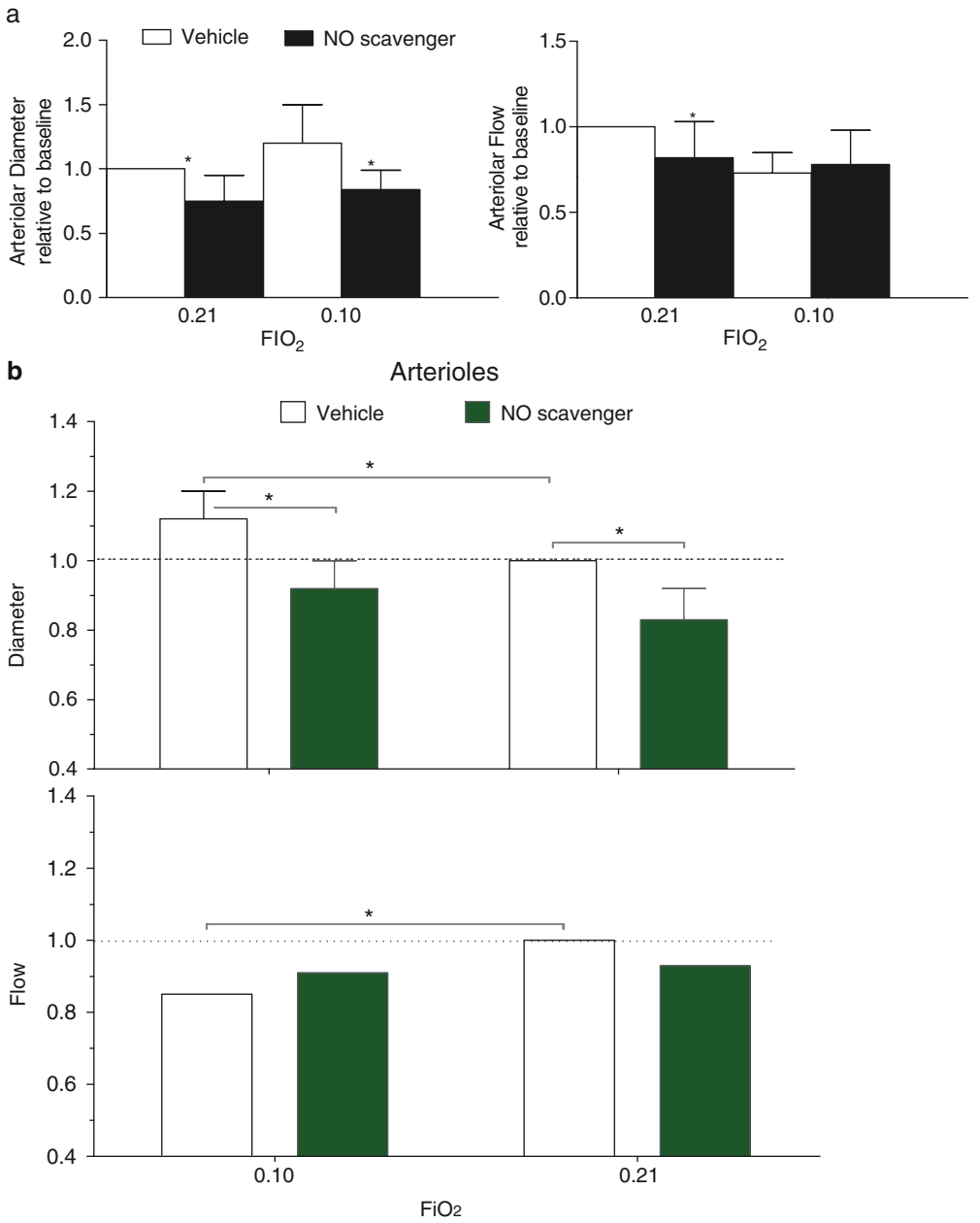

Fig. 2.1. (**a**) Changes in arteriolar hemodynamics during normoxia and hypoxia in the hamster cheek pouch microcirculation during the treatment with NO scavenger or saline (vehicle). FI_{02}, inspired oxygen fraction. Arteriolar diameters [mean (SD)] in each animal group during normoxia were as follows: NO scavenger [48.9 μm (SD 9.5), $n=35$]; vehicle [50.2 μm (SD 8.4), $n=36$]. *n* No. of vessels studied. RBC velocities [mean (SD)] in each animal group were as follows: NO scavenger [2.14 mm/s (SD 0.35)]; vehicle [2.50 mm/s (SD 1.2)]. Flows [mean (SD); $^*P<0.05$] in each animal group were as follows: NO scavenger [4.90 ηl/s (SD 3.8)]; vehicle [5.2 ηl/s (SD 7.8)]. $^*P<0.05$ vs. baseline. (**b**) Changes in arteriolar hemodynamics during normoxia, and hypoxia during the infusion of the NO scavenger (CPTIO) or saline (vehicle) in the skin fold window preparation. FI_{02}, inspired oxygen fraction. Diameters [mean (SD); $^*P<0.05$] in each animal group during normoxia were as follows: NO scavenger [56.3 μm (SD 10.2), $n=26$, $n=22$]; vehicle [58.1 μm (SD 11.4), $n=26$]. *n* No. of vessels studied. RBC velocities [mean (SD)] in each animal group were as follows: NO scavenger [4.8 mm/s (SD 1.6)]; vehicle [5.0 mm/s (SD 1.5)]. Flows [mean (SD); $^*P<0.05$] in each animal group were as follows: NO scavenger [12.2 ηl/s (SD 13.2)]; vehicle [13.0 ηl/s (SD 12.2)].

The NO scavenger and hypoxia further reduced FCD [0.71 (0.09)] to a statistically significant low when compared with normoxia and hypoxia without the NO scavenger

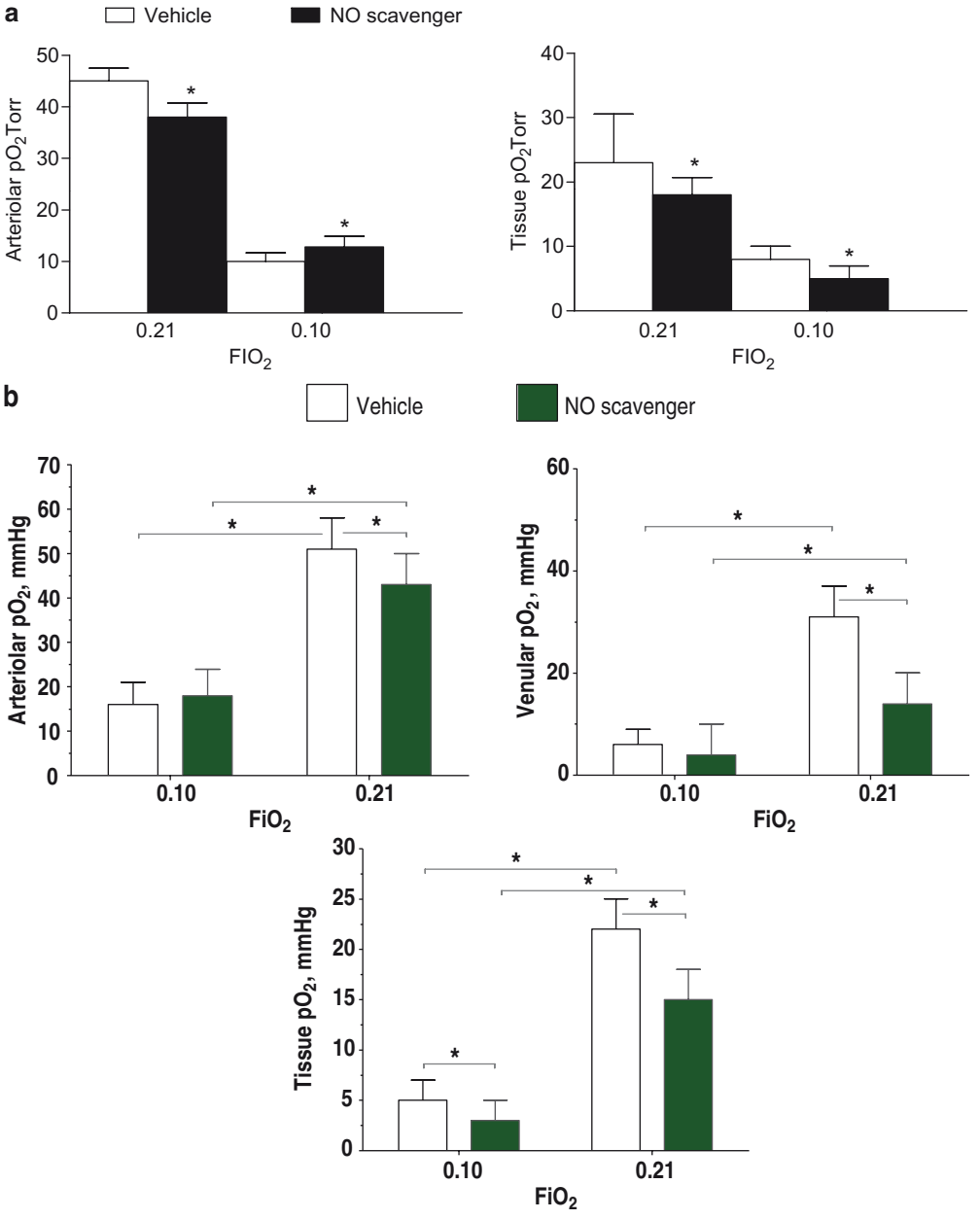

Fig. 2.2. (**a**) Microvascular oxygen distribution during normoxia and hypoxia in hamster cheek pouch with and without (CPTIO) or saline (vehicle). Values are means (SD). Each point represents an average of at least 36 measurements per group. *$\mathbf{P} < 0.05$. (**b**) Microvascular oxygen distribution during normoxia and hypoxia in skin window preparation with and without NO scavenger. Values are means (SD). Each point represents an average of at least 36 measurements per group. *$\mathbf{P} < 0.05$.

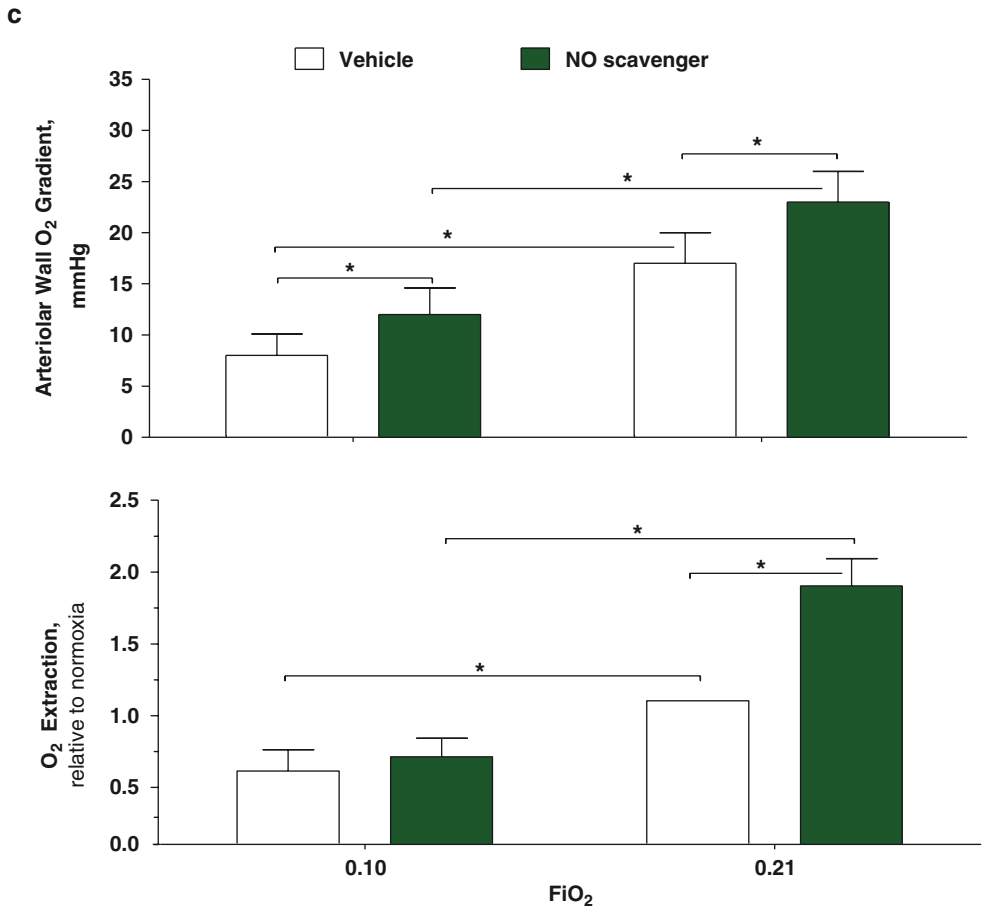

Fig. 2.2. (continued) (**c**) Microvascular oxygen distribution during normoxia and hypoxia in skin window preparation with and without NO scavenger. Values are means (SD); each point represents an average of at least 36 measurements per group. *$\mathbf{P} < 0.05$ vs. baseline.

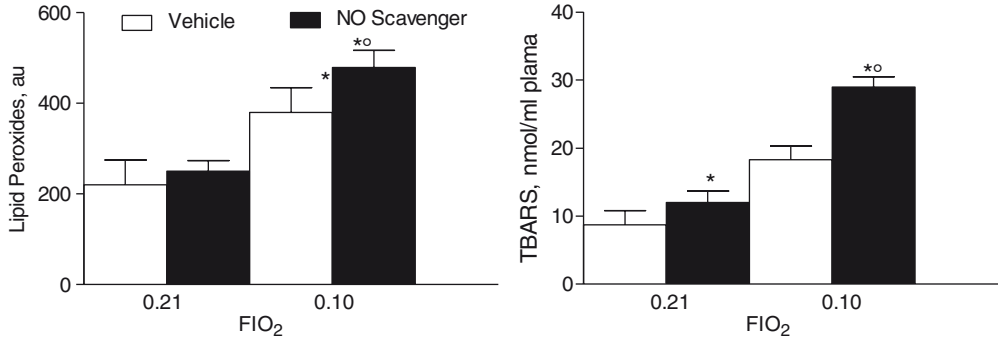

Fig. 2.3. Measurements of lipid peroxides with the two different methods, D-ROMS (*first panel*) and TBARS (*second panel*) in the systemic blood of hamsters in normoxia and hypoxia. Values are expressed as mean (±SD); $n = 7$ animals in each group. *$P < 0.05$ vs. baseline.

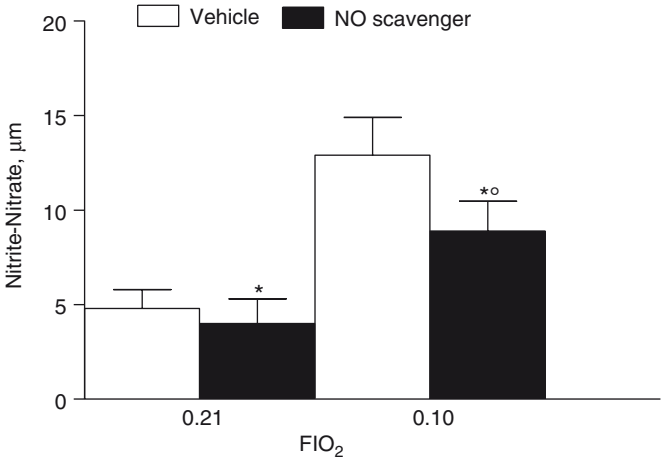

Fig. 2.4. Changes in nitrite/nitrate concentration in plasma of hamsters in normoxia and hypoxia with and without the NO scavenger. Values are means (SD); $n=7$ animals in each group. *$P<0.05$ vs. baseline.

4.3.6.2.2. Microvascular Oxygen and NO Measurement

Figure 2.2b shows the distribution of pO_2 in the microvascular arterioles and in the interstitial space (tissue) for normoxia and hypoxia, with and without the NO scavenger. Arteriolar wall gradients were determined from the difference between the intravascular and perivascular pO_2 measurements taken across the vessel wall (Fig. 2.2c). This parameter has been shown to be directly related to the rate of oxygen consumption of the vessel wall (20, 23). The vessel wall gradient in the arterioles in normoxia conditions was 16 mmHg (SD 4) [$n=10$; diameter 56 µm (SD 8)]. During the continuous infusion of the NO scavenger in normoxia, the vessel wall gradient in the arterioles was significantly increased to 23 mmHg (SD 3) [$n=12$; diameter 54 µm (SD 9)]. Hypoxia decreased the wall oxygen gradient with the NO scavenger to 11 mmHg (SD 3) [$n=8$; diameter 57 µm (SD 8)] and without the scavenger to 9 mmHg (SD 3) [$n=8$; diameter 55 µm (SD 7)]. NO concentrations were significantly increased after hypoxia and reduced after CPTIO (Fig. 2.5).

4.3.6.3. Critical Analysis of Methods

4.3.6.3.1. Oxygen Measurements

Surgical intervention, exposure to the environment, or at least, inflammation of the tissue can, in principle, increase the production of ROS/RNS as it must be assumed that these interventions and procedures should change the redox state of the membranes. However, the experimental evidence shows that the level of ROS/RNS in basal experimental conditions were low, and became significantly increased following exposure to low oxygen levels. Consequently, results from the experimental models should be representative and a consequence of the hypoxic stimulus. The analysis and measurement of oxygen distribution in the microcirculation and the tissues remains a controversial issue, primarily because there is no universally accepted method based on a common instru-

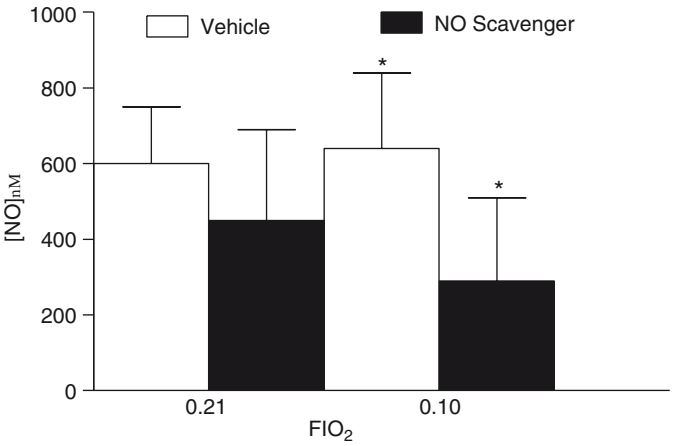

Fig. 2.5. NO concentration measured by electrode in arterioles of hamster skin fold window preparation in normoxia and hypoxia with and without the NO scavenger. Values are means (SD); $n=7$ animals in each group. *$P<0.05$ vs. normoxia.

mentation and methodology. The recent development of the phosphoresce quenching technique, although technically simple to implement, being optically based rather than using the arduous and skilful manipulation of oxygen microelectrodes, has led to both solutions and new problems. The principal new problem is that implementation with approximately similar method s in several laboratories, leads to the discovery and definition of the relative importance of mechanisms of oxygen transfer in the tissues that could not be previously evidenced. The principal problem issues on which there is no clear agreement are (1) the level of oxygen consumption by the method (2) the attainable geometrical resolution (3) the extent to which the results are affected by the toxicity of the metallo-proteins injected to obtain measurements. These features are all notably interrelated, finally leading to a significantly different understanding of the way tissue is oxygenated. There appears to be a general agreement on the validity and congruence of the measurements of intra microvascular pO_2, the concept of the longitudinal pO_2 oxygen gradient in the microcirculation having been validated by all laboratories. It is well established and functionally reasonable that the endothelium regulates the release of vasoactive substances in response to O_2 and NO availability. However, the remaining critical issues depend on the importance of O_2 consumption by the method and the magnitude of the oxygen gradients at the vessel wall. Golub et al. (51) have provided experimental evidence on the lack of significant gradients across the arteriolar wall, thus concluding that this tissue compartment is essentially transparent to the passage of oxygen, providing limited diffusional resistance and oxygen consumption. These authors indicate that the oxygen gradient at the arteriolar vascular wall is not statistically significant, and could be at most 0.5 mmHg/μ (52). A different

approach has been taken by Intaglietta et al. and Shibata et al. (15, 53), who minimized oxygen consumption by the technique, and established oxygen mass balances for the measurements, i.e., the correspondence between the longitudinal oxygen gradients correspondence with the radial rate of oxygen exit. This approach, combined with a demonstrated decreased rate of oxygen consumption show that the arteriolar wall is a significant consumer of oxygen, as evidenced by the larger that diffusion limited oxygen gradient in this district. It should be apparent that the concept of the longitudinal pO_2 gradient, or a significant oxygen exit along the microvasculature, is not compatible with the lack of a significant radial gradient in the arteriolar circulation that extracts oxygen from the blood column. It is a substantially acceptable concept to assume that the vessel wall consumes a variable but significant percentage of the available oxygen in the context of blood flow regulation.

4.3.6.3.2. ROS/RNS

Measurement of the production of ROS is difficult for several reasons. For example, in many tissues, low intracellular steady-state concentrations of superoxide occur as a result of the balance between the basal rates of partial reduction of oxygen to superoxide and the diffusion-limited scavenging of superoxide by both cytoplasmic and mitochondrial SODs, resulting in intracellular superoxide concentrations estimated to rarely exceed 1 nM (54). The extracellular release of small proportions of intracellularly formed superoxide may occur via diffusion through anion channels, and superoxide formed from plasma membrane-bound oxidases remains at relatively low levels because of the serum and extracellular fluid components, including the low molecular weight oxidant scavengers and the heparin-binding extracellular-SOD (55–57). Thus, the relatively short half-life (seconds) of ROS and the efficient and redundant systems that have evolved to scavenge them require that any detection technique must be sensitive enough to effectively compete with these intra- and extracellular antioxidant components for reaction with the substance in question. Additionally, the methods for the analysis of ROS must have adequate intracellular access to faithfully reflect intracellular conditions. Finally, the often overlapping reactivity of ROS with the detection systems may hamper unequivocal identification and quantification of the responsible substance.

4.3.6.3.3. NO Measurements

Hypoxia regulates oxygen delivery to the tissue, reducing vascular resistance in hypoxia to maintain the delivery at a constant level via signals that control the vessel tone, allowing the blood flow to vary to meet the metabolic needs (58). Hypoxia inhibits endothelial respiration in the presence of NO, rendering the endothelial cell oxygen consumption dependent on the oxygen concentration (59). The oxygen consumption by the constituents of the wall is evidenced by the difference in the pO_2 across the

arteriolar wall, or the vessel wall oxygen gradient (23). The oxygen consumption of the vessel wall and its pO_2 gradient increases because of the effect of vasoconstriction such as arginine vasopressin (42) and decreases in response to vasodilators, such as verapamil (60). The vasodilator effect of hypoxia also lowers the vessel wall oxygen consumption and the vessel wall gradient. Considering that NO synthesis has a stoichiometry of 1/1 with regard to the consumed O_2, the basal production of NO by eNOS in a rat aorta single endothelial cell requires the consumption of about 6.2×10^{-16} mol $O_2 \times s^{-1} \times cell^{-1}$ (61). Moreover, eNOS has been shown to be activated by endothelial cell stimulation with acetylcholine, leading to the activation of NO release. In the endothelium from rabbit aorta, Ach increases the NO extracellular level, and therefore, the production by ≈10 times and probably more, if the intracellular NO degradation is taken into account. Therefore, the corresponding quantity of O_2 transiently consumed by eNOS can be evaluated in the range of 10 times the basal consumption, i.e., 6.2×10^{-15} mol $O_2 \times s^{-1} \times cell^{-1}$ (62, 63). In hypoxia, the O_2 diffusion is insufficient to continuously provide O_2 as well as the enzymes, such as eNOS that consumes high levels of O_2, whereas NO modulates oxygen consumption by the tissues10, 12).

Thus, delivery of tissue oxygen is increased with NO availability because oxygen demand is reduced and vice versa. When the level of pO_2 is lower, as in hypoxia, the concentration of NO determines the tissue pO_2 and capillary perfusion.

4.4. Conclusions

In summary, our results show that reducing NO synthesis decreases the dilator response to hypoxia and tissue pO_2. Therefore, the increased NO formation reduces the O_2 consumption and decreases ROS/RNS production. Endothelial NOS while consuming oxygen, induces a significant decrease in pO_2; also, the amplitude of the consumption of oxygen by the vessel wall can be related to endothelial NOS activity. These findings may have an important implication in conditions where the NO and oxygen level decrease at the same time. Thus, the NO level in combination with decreased oxygen availability present a significant challenge to the maintenance of tissue metabolism, aggravated by the negative effects on capillary perfusion.

ROS/RNS are not simple signaling molecules but they have numerous layers of regulation to consider when assessing the outcome from possible exposure to various pO_2 tensions. NO synthesis, unlike respiration, influences intracellular oxygen tension. A complex relationship exists between the fundamental chemistry of NO and the important influences of the cellular redox state. Understanding the physiology and pathology of ROS/RNS challenges the paradigms of biological thinking and pushes the lower sensitivity limits of analytical chemistry. We conclude that it is

possible to monitor real time-NO and pO_2 dynamics under different conditions through the use of electrodes selective for NO and oxygen molecules. The importance of finding methods to measure the real in vivo concentration of NO, ROS/RNS, and oxygen is crucial because their concentrations play an important and varied role in modulating vascular injury as well as proinflammatory responses.

5. Notes

1. The phosphorescence method is based on the relationship between the decay rate of excited phosphorescence from palladium_mesotetra_(4_carboxyphenyl)porphyrin bound to albumin and the partial pressure of oxygen, according to the Stern_Volmer equation . In this method, animals receive a slow intravenous injection of the porphyrin dye (15 mg/kg body wt) at a concentration of 10 mg/ml approximately 10 min before pO_2 measurements. The dye is made to phosphoresce by excitation with light flashes, and the oxygen concentration in an adjustable optical window that delineates the area where the measurement is to be made, is deduced from the rate of decay of the phosphorescence, which depends on the amount of oxygen that surrounds the dye. Phosphorescence is the emission of photons due to the electronic transition in molecules that are excited into a triplet state by absorbing light and then the transition from this state to a singlet ground state. Molecules such as Pd-porphyrin either release the absorbed energy as light or transfer this energy to oxygen, which prevents light emission, thus "quenching" the phosphorescence. The intensity of light emission $I(t)$ from many molecules is described by an exponential decay of the form: $I(t) = I_0 \exp(-t/a)$ where I_0 is the maximum intensity at $t = 0$ and a is the decay time constant. When light emission is quenched, fewer photons are emitted, which translates into a shorter time constant a. For quenching to occur, it is necessary that the phosphorescent molecule and the quenching agent (oxygen) collide before the occurrence of the triplet to ground state transition, a process that is, in part, dependent on the abundance (or concentration) of quenchers. The relationship between the decay constant a and the oxygen concentration (given by the product of oxygen solubility in the medium, $\forall$, and the local partial pressure pO_2 of oxygen) is given by the Stern–Volmer equation $J_0/a = 1 + K_Q\ J_0\ \forall\ pO_2$, where J_0 is the phosphorescence decay constant in the absence of oxygen, and K_Q is the quenching constant. An advantage of this method is that mixing Pd-porphyrin with excess albumin leads to the formation of a probe whose sensitivity to oxygen

quenching is independent of the probe concentration. In other words, the decay constant becomes independent of the concentration of the albumin/porphyrin complex.

2. The phosphorescence generated by the light excitation of the porphyrin probe consumes O_2. The amount consumed depends upon the concentration of the dye and the total energy delivered by the light source. With a very intense illumination, it is possible to make a determination of the oxygen level with a single flash. In this implementation, the flash lamp employed had a 25 s decay constant, which precluded the acquisition of phosphorescence decay data prior to about 80 s after flash extinction, and therefore, prevented reliable measurements of pO_2 above about 50 mmHg, which corresponds to a phosphorescence decay time of similar duration. The emission obtained with this technique is intense, and the phosphorescence decay curve may be the summation of signals from adjoining areas that would not normally have sufficient intensity to affect the principal component present, particularly if the measurement is made in the neighborhood of microvessels where the oxygen field is not uniform. In addition, oxygen is consumed as the phosphorescence decays, further distorting the decay signal. These problems have been reported to be amenable to solution by deconvolving the decay signal using mathematical techniques, an approach that may be useful if the signal noise is very small.
3. All implementations use a probe injection of 20–30 mg porphyrin/kg bw, leading to a blood concentration of 0.3 mg/ml, and a tissue fluid concentration smaller than 0.1 mg/ml. The multi-flash system of Torres Filho and Intaglietta with a flash decay constant of 10 s requires 100 flashes to obtain an interpretable signal in blood, each flash consuming oxygen, causing the concentration of oxygen in stationary plasma to decrease by 0.01 mmHg/flash at steady state. Thus, a single flash system that gives an interpretable signal will introduce an error <1 mmHg when used in stationary tissue fluid. This error may be lower in tissue because the amount of probe present is about 1/3 that of plasma; but this causes a proportional decrease in phosphorescence signal, requiring a significant increase of flash intensity and a corresponding increase in the consumption of oxygen, which may explain why not all systems are able to obtain tissue measurements. Comparison of in vivo pO_2 measurements at the same site with the multi-flash phosphorescence method and the microelectrode technique were obtained by two groups of investigators using avascular tissue areas of the hamster skin fold preparation and rat skeletal muscle. In the hamster preparation superfused with Krebs solution bubbled with 100% N_2, there was a maximum divergence of 2% between the methods over the tissue pO_2 range of 5–40 mmHg.

References

1. Haliwell B, Gutteridge JMC (1999) Free radical in Biology and Medicine. Oxford University Press, London
2. Dröge W (2001) Free radicals in the physiological control of cell function. Physiol Rev 82:47–95
3. Halliwell B, Gutteridge JMC (1985) The chemistry of oxygen radicals and other oxygen-derived species. In: Free radicals in biology and medicine. Oxford University Press, New York, pp 20–64
4. Barreto JC, Smith GS, Stobel NHP, McQuillin PA, Miller TA (1995) Teraphtalic acid: a dosimeter for detection of hydroxyl radical in vitro. Life Sci 56:89–96
5. Parker L (ed) (1994) Oxygen radicals in biological systems. In: Methods in Enzymology, vol 234, part D. Academic, New York
6. Ignarro LJ (2002) Nitric oxide is an unique signaling molecule in the vascular system: a historical overview. J Physiol Pharmacol 53: 503–514
7. Buerk DG (2007) Nitric oxide regulation of microvascular oxygen. Antioxid Redox Signal 9:829–843
8. Abu-Soud HM, Rousseau DL, Stuehr DJ (1966) Nitric oxide binding to the heme of neuronal nitric-oxide synthase links its activity to changes in oxygen tension. J Biol Chem 271:32515–32518
9. Bertuglia S, Giusti A (2005) The role of nitric oxide in capillary perfusion and oxygen delivery regulation during systemic hypoxia. Am J Physiol Heart Circ Physiol 288(2):H525–531
10. Shen W, Xu X, Ochoa M, Zhao G, Wolin MS, Hintze TH (1994) Role of nitric oxide in the regulation of oxygen consumption in conscious dogs. Circ Res 75:1086–1095
11. King CE, Melinyshyin MJ, Mewburn JD, Curtis SE, Winn MJ, Cain SM, Chapler CK (1994) Canine hindlimb flow and O_2 uptake after inhibition of EDRF/NO synthesis. J Appl Physiol 76:1166–1171
12. Cabrales P, Tsai AG, Intaglietta M (2006) Nitric oxide regulation of microvascular oxygen exchange during hypoxia and hyperoxia. J Appl Physiol 100:1181–1187
13. Stamler JS (1995) S-nitrosothiols and the bioregulatory actions of nitrogen oxides through reactions with thiol groups. Curr Top Microbiol Immunol 196:19–36
14. Jia L, Bonaventura C, Bonaventura J, Stamler JS (1996) S-nitrosohaemoglobin: a dynamic activity of blood involved in vascular control. Nature 380:221–226
15. Intaglietta M, Johnson PC, Winslow RM (1996) Microvascular and tissue oxygen distribution. Cardiovasc Res 32:632–643
16. Hogan MC (1999) Phosphorescence quenching method for measurement of intracellular pO_2 in isolated skeletal muscle fibers. J Appl Physiol 86:720–724
17. Kessler M, Harrison, DK, Hoper J (1986) Tissue oxygen measurement techniques. In: Baker CH, Nastuk WL, Orlando FL (eds) Microcirculatory technology. Academic, New York, pp. 391–425
18. Popel AS, Pittman RN, Ellsworth ML (1989) Rate of oxygen loss from arterioles is an order of magnitude higher than expected. Am J Physiol 256:H921–H924
19. Tsai AG, Johnson PC, Intaglietta M (2003) Oxygen gradients in the microcirculation. Physiol Rev 83:933–963
20. Kerger H, Saltzman DJ, Gonzales A, Tsai AG, van Ackern K, Winslow RM, Intaglietta M (1997) Microvascular oxygen delivery and interstitial oxygenation during sodium pentobarbital anesthesia. Anesthesiology 86:372–386
21. Pawlowski M, Wilson DF (1992) Monitoring of the oxygen pressure in the blood of live animals using the oxygen dependent quenching of phosphorescence. Adv Exp Med Biol 316:179–185
22. Sinaasappel M, van Iterson M, Ince C (1992) Microvascular oxygen pressure in the pig intestine during hemorrhagic shock and resuscitation. J Physiol (Lond) 514:245–253
23. Tsai AG, Friesenecker B, Mazzoni MC, Kerger H, Buerk DG, Johnson PC, Intaglietta M (1988) Microvascular and tissue oxygen gradients in the rat mesentery. Proc Natl Acad Sci USA 95:6590–6595
24. Wilson DF (1993) Measuring oxygen using oxygen dependent quenching of phosphorescence: a status report. Adv Exp Med Biol 333:225–232
25. Seylaz E, Pinard J (1977) Continuous intracerebral PO2 and PCO2 measurements by mass spectrometry: study of the influence of vasoactive drugs. Acta Neurol Scand 64: 438–439
26. Grisham MB (1994) Oxidants and free radicals in inflammatory bowel disease. Lancet 344: 859–861
27. Pryor WA, Stanley JP, Blair E (1976) Autoxidation of polyunsaturated fatty acids: II. A suggested mechanism for the formation of TBA-reactive materials from prostaglandin-like endoperoxides. Lipids 11:370–379

28. Bertuglia S, Reiter NJ (2007) Melatonin reduces ventricular arrhythmias and preserves capillary perfusion during ischemia-reperfusion events in cardiomyopathic hamsters. J Pineal Res 42(1):55–63
29. Salvemini D, Mazzon E, Dugo L, Serraino I, De Sarro A, Caputi AP, Cuzzocrea S (2001) Amelioration of joint disage in a rat model of collagen-induced arthritis in M40403, a superoxide dismutase mimetic. Arthritis Rheum 44:2909–2291
30. Szabo A, Hake P, Salzman AL, Szabo C (1999) Beneficial effects of mercaptothylguanidine, an inhibitor of the inducible isoform of NO synthase and a scavenger of peroxinitrite in a porcine model of delayed hemorrhagic shock. Crit Care Med 27:1343–1359
31. Halliwell B, Gutteridge JMC (2000) Detection of free radicals and other reactive species: trapping and finger printing. In: Halliwell B, Gutteridge JMC (eds) Free Radicals in Biology and Medicine. Oxford University Press, Oxford, pp 351–429
32. Morrow JD, Hill KE, Burk RF, Nammour TM, Badr KF, Roberts LJ (1990) A series of prostaglandin F2-like compounds are produced in vivo in humans by a non-cyclooxygenase, free radical-catalyzed mechanism. Proc Natl Acad Sci USA 87:9383–9387
33. Wink DA, Kim S, Coffin D, Cook JC, Vodovotz Y, Chistodoulou D, Jourd'heuil D, Grisham MB (1999) Detection of S-nitrosothiols by fluorometric and colorimetric methods. Methods Enzymol 301:201–211
34. Karlsson J (1997) Introduction to nutraology and radical formation. In: Antioxidants and exercise. Human Kinetics Press, Illinois, pp 1–143
35. Baker JE, Froncisz W, Joseph J, Kalyanaraman B (1997) Spin label oximetry to assess extracellular oxygen during myocardial ischemia. Free Radic Biol Med 22:109–115
36. Velan SS, Spencer RG, Zweier JL, Kuppusamy P (2000) Electron paramagnetic resonance oxygen mapping (EPROM): direct visualization of oxygen concentration in tissue. Magn Reson Med 43:804–809
37. Acworth IN, Bailey B (1997) Reactive oxygen species. In: The handbook of oxidative metabolism. ESA, Northampton, MA, pp 1–4.
38. Bertuglia S, Colantuoni A, Coppini G, Intaglietta M (1991) Hypoxia- or hyperoxia-induced changes in arteriolar vasomotion in skeletal muscle microcirculation. Am J Physiol 260:H362–H372
39. Bertuglia S, Giusti A, Del Soldato P (2004) Antioxidant activity of a nitro derivative of aspirin against ischemia reperfusion in hamster cheek pouch microcirculation. Am. J. Physiol. Gastrointestinal-Liver Physiol. 286(3):G437–G443
40. Bertuglia S, Giusti A (2003) Microvascular oxygenation, oxidative stress, nitric oxide suppression and superoxide dismutase during postischemic reperfusion. Am J Physiol 285:H1064–H1071
41. Cabrales P, Tsai AG, Intaglietta M (2004) Increased tissue PO_2 and decreased O_2 delivery and consumption after 80% exchange transfusionwith polymerized hemoglobin. Am J Physiol Heart Circ Physiol 287:H2825–H2833
42. Friesenecker B, Tsai AG, Dunser MW, Mayr AJ, Martini J, Knotzer H, Hasibeder W, Intaglietta M (2004) Oxygen distribution in the microcirculation following arginine vasopressin-induced arteriolar vasoconstriction. Am J Physiol Heart Circ Physiol 287:H1792–H1800
43. Torres Filho IP, Intaglietta M (1993) Microvessel PO_2 measurement by phosphorence decay method. Am J Physiol Heart Circ Physiol 265:H1537–H1545
44. Kerger H, Groth G, Kalenka A, Vajkoczy P, Tsai AG, Intaglietta M (2003) PO_2 measurements by phoroshorence quenching characteristics and applications of an automated system. Microvasc Res 15:93–101
45. Friedemann MN, Robinson SW, Gerhardt GA (1996) o-Phenylenediamine-modified carbon fiber electrodes for the detection of nitric oxide. Anal Chem 68:2621–2628
46. Cabrales P, Tsai AG, Intaglietta M (2004) Microvascular pressure and functional capillary density in extreme hemodilution with low and high plasma viscosity expanders. Am J Physiol Heart Circ Physiol 287:H363–H373
47. Tsai AG, Acero C, Nance PR, Frangos JA, Buerk DG, Intaglietta M (2005) Elevated plasma viscosity in extreme hemodilution increases perivascular nitric oxide concentration and microvascular perfusion. Am J Physiol Heart Circ Physiol 288:H1730–H1739
48. Sarelius IH (1968) Cell flow path influences transit time through striated muscle capillaries. Am J Physiol Heart Circ Physiol 250:H899–H907
49. Bohlen HG, Nase GP (2000) Dependence of intestinal arteriolar regulation on flow-mediated nitric oxide formation. Am J Physiol Heart Circ Physiol 279:H2249–H2258
50. Grishman MB, Jonshon GG, Lancaster JR (1966) Quantitation of nitrite and nitrate in extracellular fluids. Methods Enzymol 268:237–246

51. Golub AS, Barker MG, Pittman RN (2007) PO_2 profiles near arterioles and tissue oxygen consumption in rat mesentery. Am J Physiol Heart Circ Physiol 293:H1097–H1106
52. Golub AS, Pittman RN (2008) PO_2 measurements in the microcirculation using phosphorescence quenching microscopy at high magnification. Am J Physiol Heart Circ Physiol 294:H2095–H2916
53. Shibata M, Ichioka S, Ando J, Kamiya A (2001) Microvascular and interstitial PO_2 measurements in rat skeletal muscle by phosphorence quenching. J Appl Physiol 91:321–327
54. Tarpey MM, Wink DA, Grishman MB (2008) Methods for detection of reactive metabolites of oxygen and nitrose: in vitro and in vivo considerations. Am J Physiol Regul Integr Comp Physiol 206:R431–R444
55. Halliwell B (1995) How to characterize an antioxidant: an update. Biochem Soc Symp 61:73–101
56. Rice-Evans CA, Diplock AT (1993) Current status of antioxidant therapy. Free Radic Biol Med 15:77–96
57. Skulachev VP (1997) Membrane-linked systems preventing superoxide formation. Biosci Rep. 17:347–366.
58. Prewitt RL, Johnson PC (1976) The effect of oxygen on arteriolar red cell velocity and capillary density in the rat cremaster muscle. Microvasc Res 12:59–70
59. Edmunds NJ, Marshall JM (2003) The roles of nitric oxide in dilating proximal and terminal arterioles of skeletal muscle during systemic hypoxia. J Vasc Res 40:68–76
60. Hangai-Hoger N, Tsai AG, Friesenecker B, Cabrales P, Intaglietta M (2005) Microvascular oxygen delivery and consumption following treatment with verapamil. Am J Physiol Heart Circ Physiol 288:H1515–H1520
61. Akaike T, Yoshida M, Miyamoto Y (1993) Antagonistic action of imidazolineoxyl N-oxides against endothelium-derived relaxing facto/ NO through a radical reaction. Biochemistry 32:827–832
62. Christie MI, Griffith TM, Lewis MJ (1989) A comparison of basal and agonist-stimulated release of endothelium-derived relaxing factor from different arteries. Br J Pharmacol 98:397–406
63. Coste J, Vial JC, faury G, Deronzier A, Usson Y, Nicoud MR, Verdetti J (2002) NO synthesis, unlike respiration, influences intracellular oxygen tension. Biochem Biophys Res Comm 209:97–104

http://www.springer.com/978-1-60761-410-4

Advanced Protocols in Oxidative Stress II
Armstrong, D. (Ed.)
2010, XIV, 444 p., Hardcover
ISBN: 978-1-60761-410-4
A product of Humana Press